Epoxide as a precursor to secondary organic aerosol formation from isoprene photooxidation in the presence of nitrogen oxides

Ying-Hsuan Lin[a], Haofei Zhang[a,1], Havala O. T. Pye[b], Zhenfa Zhang[a], Wendy J. Marth[a], Sarah Park[a], Maiko Arashiro[a], Tianqu Cui[a], Sri Hapsari Budisulistiorini[a], Kenneth G. Sexton[a], William Vizuete[a], Ying Xie[b], Deborah J. Luecken[b], Ivan R. Piletic[b], Edward O. Edney[b], Libero J. Bartolotti[c], Avram Gold[a], and Jason D. Surratt[a,2]

[a]Department of Environmental Sciences and Engineering, Gillings School of Global Public Health, University of North Carolina at Chapel Hill, Chapel Hill, NC 27599; [b]National Exposure Research Laboratory, Office of Research and Development, US Environmental Protection Agency, Research Triangle Park, NC 27711; and [c]Department of Chemistry, East Carolina University, Greenville, NC 27858

Edited by Mark H. Thiemens, University of California at San Diego, La Jolla, CA, and approved February 22, 2013 (received for review December 16, 2012)

Isoprene is a substantial contributor to the global secondary organic aerosol (SOA) burden, with implications for public health and the climate system. The mechanism by which isoprene-derived SOA is formed and the influence of environmental conditions, however, remain unclear. We present evidence from controlled smog chamber experiments and field measurements that in the presence of high levels of nitrogen oxides (NO_x = NO + NO_2) typical of urban atmospheres, 2-methyloxirane-2-carboxylic acid (methacrylic acid epoxide, MAE) is a precursor to known isoprene-derived SOA tracers, and ultimately to SOA. We propose that MAE arises from decomposition of the OH adduct of methacryloylperoxynitrate (MPAN). This hypothesis is supported by the similarity of SOA constituents derived from MAE to those from photooxidation of isoprene, methacrolein, and MPAN under high-NO_x conditions. Strong support is further derived from computational chemistry calculations and Community Multiscale Air Quality model simulations, yielding predictions consistent with field observations. Field measurements taken in Chapel Hill, North Carolina, considered along with the modeling results indicate the atmospheric significance and relevance of MAE chemistry across the United States, especially in urban areas heavily impacted by isoprene emissions. Identification of MAE implies a major role of atmospheric epoxides in forming SOA from isoprene photooxidation. Updating current atmospheric modeling frameworks with MAE chemistry could improve the way that SOA has been attributed to isoprene based on ambient tracer measurements, and lead to SOA parameterizations that better capture the dependency of yield on NO_x.

air pollution | anthropogenic | biogenic | particulate matter | fine aerosol

Isoprene (2-methyl-1,3-butadiene, C_5H_8) is released by terrestrial vegetation in an estimated quantity of 600 teragram-yr^{-1} (Tg-yr^{-1}) (1) and represents the largest single nonmethane hydrocarbon emission into Earth's atmosphere. Photooxidation of isoprene by hydroxyl radicals (OH) during the daytime (2) has been identified as a source of tropospheric ozone (O_3) (3) and secondary organic aerosol (SOA) (4–11). Recent work has shown that anthropogenic pollutants, particularly mixtures of nitrogen oxides (NO_x = NO + NO_2) and sulfur dioxide (SO_2), greatly enhance isoprene as a source of SOA (5, 6, 8, 10, 11). While isoprene is thought to be a substantial contributor to global SOA (12, 13), the mechanism by which isoprene-derived SOA is formed and the influence of environmental conditions on SOA formation remain unclear, but are critical to developing $PM_{2.5}$ control strategies for protection of public health and to assessing the impact on the climate system. Community Multiscale Air Quality (CMAQ) model simulations indicate that removal of controllable anthropogenic emissions could affect a reduction of greater than 50% in biogenic SOA in the eastern United States (14).

NO_x-dependent chemical pathways have been proposed to explain isoprene-derived SOA tracers common to both laboratory-generated and organic aerosols in atmospheres typical of the urban environment (15). SOA formation from isoprene under high-NO_x conditions has been ascribed to the oxidation of methacryloylperoxynitrate (MPAN) (10, 16), which laboratory studies have established as a second-generation oxidation product of isoprene (17, 18). High NO_2/NO ratios favor formation of MPAN from both isoprene and methacrolein (MACR) photooxidation and result in enhanced SOA yields (10, 16). Identification of similar chemical constituents in SOA produced from the photooxidation of isoprene, MACR, and MPAN further supports the central role of MPAN oxidation under these conditions (10). Mass spectrometric analysis of oligoesters and their mono nitrated and sulfated derivatives from SOA generated in the high NO_2/NO chamber experiments yields a series of product ions separated by 102 Da, suggesting a common monomeric unit. While a mechanism of oligoester formation remains to be determined, the observation of a common monomeric unit is in accord with a critical single gas-phase intermediate from MPAN photooxidation as an oligoester precursor (10).

The mechanism proposed in Fig. 1 for SOA formation from the photooxidation of isoprene in the presence of NO_x shows the published route to MPAN via the H-abstraction channel of the branching reaction of MACR with OH (17–19). The fate of the transient resulting from the addition of OH to MPAN, however, has until recently been a matter of conjecture. Kjaergaard et al. (20) have reported a computational study suggesting that the transient OH adduct of MPAN (HOMPAN) reacts by elimination of nitrate radical (NO_3) followed by an intramolecular rearrangement to hydroxymethylmethyl-α-lactone (HMML), which is suggested as the precursor of known high-NO_x SOA compounds and oligoesters. In Fig. 1 we suggest a second parallel, thermodynamically feasible pathway via rearrangement of HOMPAN to methacrylic acid epoxide (MAE), which yields known high-NO_x SOA marker compounds and oligoesters similar to those previously reported from photooxidation of isoprene, MACR, and MPAN (10, 16, 21). This study presents experimental evidence supported by computational and modeling studies that the most

Author contributions: Y.-H.L., H.Z., H.O.T.P., E.O.E., L.J.B., A.G., and J.D.S. designed research; Y.-H.L., H.Z., H.O.T.P., Z.Z., W.J.M., S.P., M.A., T.C., S.H.B., K.G.S., Y.X., D.J.L., I.R.P., E.O.E., L.J.B., A.G., and J.D.S. performed research; Y.-H.L., H.Z., H.O.T.P., Z.Z., W.V., D.J.L., E.O.E., L.J.B., A.G., and J.D.S. analyzed data; and Y.-H.L., H.Z., H.O.T.P., E.O.E., L.J.B., A.G., and J.D.S. wrote the paper.

The authors declare no conflict of interest.

This article is a PNAS Direct Submission.

Freely available online through the PNAS open access option.

[1]Present address: Lawrence Berkeley National Laboratory, Berkeley, CA 94720.

[2]To whom correspondence should be addressed. E-mail: surratt@unc.edu.

This article contains supporting information online at www.pnas.org/lookup/suppl/doi:10.1073/pnas.1221150110/-/DCSupplemental.

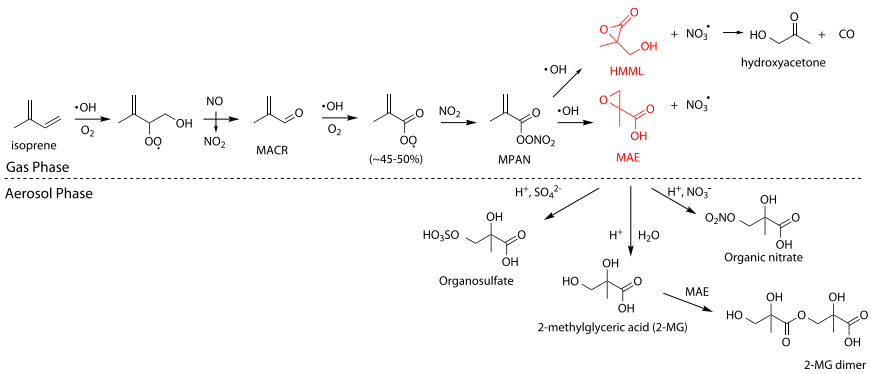

Fig. 1. Proposed mechanism for SOA formation from isoprene photooxidation in the presence of NO_x.

likely route for isoprene-derived SOA under high-NO_x conditions is via the gas-phase intramolecular rearrangement of the HOMPAN adduct to MAE followed by reactive uptake. We have detected gaseous MAE in the local environment, and modeling of MAE production on a local scale is in accord with measured concentrations. Chemical transport modeling of ambient concentrations of gaseous MAE on a large scale over the continental United States demonstrates a potentially significant contribution of MAE to SOA in regions where isoprene emissions interact with anthropogenic pollutants. Taken together, the results present a coherent picture that strongly supports MAE as a critical intermediate leading to SOA formation from isoprene photooxidation in the presence of NO_x and fills in an important step in the pathway to SOA under conditions where biogenic and anthropogenic emissions interact.

Results and Discussion

MAE from the Photooxidation of MACR in Presence of NO_x. The photooxidation of MACR to MAE is confirmed by controlled outdoor smog chamber experiments conducted under the irradiation of natural sunlight at ambient temperature in the presence of NO_x. Initial concentrations of MACR [1 part per million by volume (ppmv)], NO [400 parts per billion by volume (ppbv)], and NO_2 (200 ppbv) were set for optimization of MPAN formation and generation of sufficient oxidation products for off-line chemical analysis based on simulations from a one-dimensional box model (*SI Text*). Gas-phase samples were collected hourly with two fritted glass bubblers connected in series and preceded by a Teflon filter to remove aerosol. Ethyl acetate was selected as an aprotic collection solvent to avoid the possibility of MAE hydrolysis, and the collection train was cooled in an ice bath to minimize the evaporation of solvent and volatile products. The bubbler samples were analyzed by ultra performance liquid chromatography interfaced to a high-resolution quadrupole time-of-flight mass spectrometer equipped with an electrospray ionization source (UPLC/ESI-HR-Q-TOFMS) operated in the negative ion mode. The extracted ion chromatograms (EICs) at the nominal mass of the MAE anion, *m/z* 101, are compared in Fig. 2. The EIC in Fig. 2*A* is from a MACR/NO_x photooxidation experiment and in Fig. 2*B* from an authentic MAE standard in ethyl acetate, which both show a single major peak with an identical retention time. The accurate mass of the extracted ion at *m/z* 101 corresponds to the composition of the MAE anion ($C_4H_5O_3^-$) within ± 1 mDa for both the bubbler sample and the MAE standard.

The quantitative time profile of MAE formation during the course of an MACR photooxidation experiment (Fig. S1) shows that the increase in gaseous MAE tracks with particle nucleation and growth. Since no seed aerosol was introduced into the chamber before the experiment, the increase of aerosol mass concentration can be ascribed to nucleation of MAE followed by heterogeneous oxirane ring-opening reactions. Off-line UPLC/ESI-HR-Q-TOFMS analysis of the nucleated aerosol collected on the Teflon filter preceding the tandem bubblers is in accord with this contention. The collected material is comprised primarily of higher order oligoesters with MAE as a common monomeric unit (Table S1), consistent with the high-NO_x MPAN SOA constituents reported in Surratt et al. (10) and high-NO_x MACR SOA constituents reported by other investigators (16, 22), and thus consistent with MAE as the intermediate involved in SOA formation in these experiments.

Gas chromatography/flame ionization detection data indicated that complete reaction of MACR was coincident with peak MAE concentration (Fig. S1), and analysis of the back-up bubbler for breakthrough indicated a collection efficiency of 86% for gas-phase MAE. MAE rapidly converts to particle mass, and assuming MAE contributes 50–80% of the measured SOA mass in the chamber experiment (8), a range of values for the chamber-based MAE yield was determined. The total MAE mass concentration profile was estimated by summing the mass concentrations of MAE in the particle and gas phases as a function of time for the 50% and 80% contributions. For each total mass contribution, an initial value for the MAE yield was selected and the time profile of the MAE concentration computed using the Statewide Air Pollution Research Center-07 (SAPRC07) chemical mechanism in a one-dimensional box model to obtain the

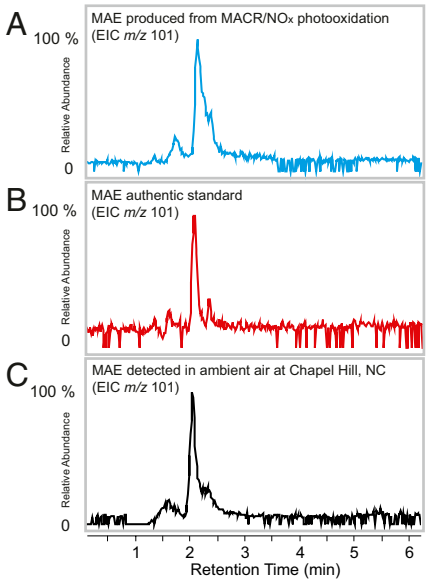

Fig. 2. Gaseous MAE detected by UPLC/(–)ESI-HR-Q-TOFMS from (*A*) an irradiated MACR/NO_x outdoor smog chamber experiment, (*B*) authentic MAE standard, and (*C*) an ambient air sample collected in Chapel Hill, North Carolina, during summer 2012.

molar yield of MAE. The procedure was repeated, varying the MAE yield until the predicted MAE mass concentration time profile was in agreement with the chamber profile (Fig. S2). The final MAE yields for the 50% and 80% mass contributions provide lower and upper bounds of 0.18 and 0.32, respectively, for the reaction of OH + MPAN to form MAE (see *SI Text* for further details).

Reactive Uptake of MAE onto Acidified Sulfate Aerosol. The Kleindienst et al. (23) tracer-based source apportionment method uses 2-methylglyceric acid (2-MG) as an isoprene SOA tracer. We are able to provide insight into the mechanism of 2-MG formation by dark reactive uptake of MAE onto preexisting seed aerosols (Table S2). Fig. S3 demonstrates that the uptake of synthetic MAE onto acidified sulfate aerosols yields substantial SOA mass, while uptake onto preexisting neutral sulfate seed aerosol is negligible. Fig. 3 shows that 2-MG is a component of SOA formed from the reactive uptake of MAE onto preexisting acidified sulfate aerosol and has also been identified in SOA generated by the photochemical oxidation of both isoprene and MACR in the presence of NO_x, and in $PM_{2.5}$ collected from downtown Atlanta, Georgia, on August 9, 2008, at an $[NO_2]/[NO]$ ratio of 5.14 (22). Other high-NO_x SOA tracers, such as the sulfate ester of 2-MG (Fig. S4), as well as the 2-MG dimer (24), have also been observed in these systems. The origin of the markers is most readily explained via nucleophilic attack on the oxirane ring of MAE by water to yield 2-MG, SO_4^{2-} to yield 2-MG sulfate, or the carboxylate anion of MAE to yield the 2-MG dimer. Formation of sulfates and oligoesters by acid-catalyzed esterification is kinetically unfavorable under tropospheric conditions (25), and therefore ruled out as a mechanism.

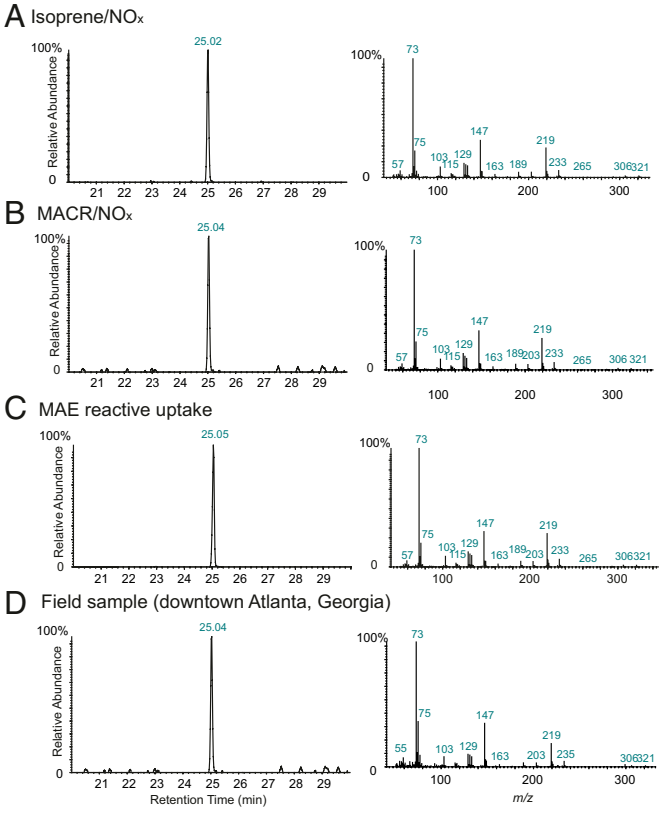

Fig. 3. EICs of *m/z* 119 from gas chromatography/electron impact mass spectrometry traces and corresponding mass spectra showing the presence of 2-MG in aerosol collected from (*A*) an isoprene/NO_x photooxidation experiment, (*B*) an MACR/NO_x photooxidation experiment, (*C*) a dark reactive uptake study of MAE, and (*D*) an ambient $PM_{2.5}$ sample from downtown Atlanta, Georgia.

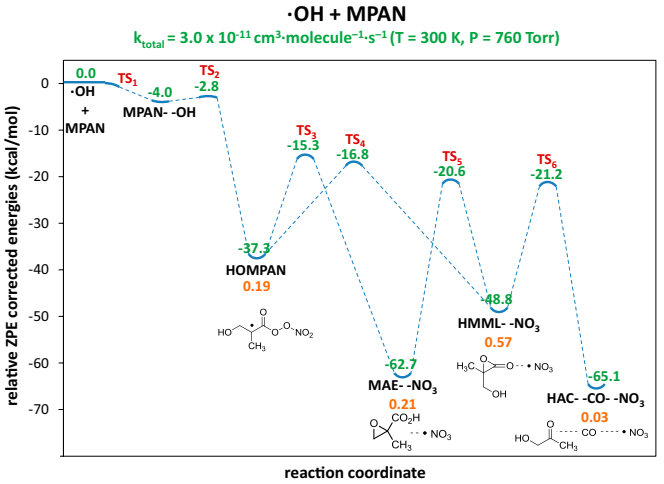

Fig. 4. Relative zero point energy (ZPE)-corrected energies (green) and product yields (orange) for the reaction of MPAN with OH calculated at m062×/maug-cc-pvtz level of theory. Results are shown for the adjusted value of -2.80 kcal·mol^{-1} for the TS_2 transition state energy.

SOA yields (mass of SOA formed/initial MAE concentration) from our reactive uptake experiments are not reported because the uptake behavior of MAE is beyond the scope of the thermal equilibrium partitioning approach, and involves competitive kinetics. Additional work is required to obtain the reactive uptake coefficients (or reaction probabilities, γ) to determine the heterogeneous removal rate of MAE. The heterogeneous removal rate will likely be highly variable, depending on particle composition, phase, acidity, presence of surfactants, and liquid water content. Once the heterogeneous removal rate has been determined, the current modeling framework can be refined to represent MAE chemistry in SOA models with increased accuracy.

Computational Investigations of the OH + MPAN Reaction Pathway. As a first step in developing a chemical mechanism for the OH + MPAN addition reaction to form SOA from photooxidation of MACR in the presence of NO_x, calculations were carried out to estimate the total rate constant for this reaction and the yields of its products, including MAE. The energy diagram in Fig. 4 was constructed based on our laboratory and field investigations of the formation of MAE from MACR under high-NO_x conditions and the recent report of Kjaergaard et al. (20) on the potential formation of HMML from OH + MPAN. The quantum chemistry codes GAUSSIAN 2009, a nudged elastic band (NEB) approach for identifying minimum energy paths, complexes, and transition states, and DIMER for refining transition states and their energies were used to construct the energy diagram (26–29). All of the quantum chemistry calculations were performed with the m062× density functional in GAUSSIAN 2009, using initially the 6–311++g** orbital basis set.

The energy diagram shows the loose and tight transition states and, as products, the MPAN–OH van der Waals complex, the HOMPAN adduct, and the loosely bound complexes MAE–NO_3, HMML–NO_3, and HAC (hydroxy acetone)–CO–NO_3. The first NEB calculation, carried out between OH + MPAN and HOMPAN, revealed a barrierless potential energy curve connecting the loose transition state TS_1, the MPAN–OH van der Waals complex and the tight transition state TS_2. A second NEB calculation between HOMPAN and HAC–CO–NO_3 showed HMML–NO_3, along with the tight TS_4 and TS_6 transition states connecting HOMPAN to HMML–NO_3 and HMML–NO_3 to HAC–CO–NO_3, respectively. Since MAE–NO_3 was an expected intermediate in this reaction, a third NEB calculation was set

up between HOMPAN and HAC–CO–NO_3, but this time with MAE–NO_3 as an intermediate in the initial trajectory. The results of this NEB calculation confirmed the presence of MAE–NO_3 and HMML–NO_3 as well as the tight TS_3, TS_5, and TS_6 transition states. The energy minima in Fig. 4 corresponding to OH + MPAN, MPAN–OH, HOMPAN, MAE–NO_3, HMML–NO_3, and HAC–CO–NO_3 were refined by computing their structures, energies, and vibrational frequencies using the maug-cc-pvtz basis set (30). The same level of theory was used by DIMER to improve those properties for the tight transition states. The optimized zero point energy-corrected electronic energies relative to the OH + MPAN energy for MPAN–OH, HOMPAN, MAE–NO_3, HMML–NO_3, HAC–CO–NO_3, and the tight transition states are shown in the diagram.

The structures, vibrational frequencies, and energies of the reactants and the tight transition states, the fitted Morse parameters for the barrierless potential energy curve, the average energy transfer parameter, and the Lennard–Jones parameters were used as input for VARIFLEX, a widely used chemical kinetics code (31–33), to compute the total rate constant and molar yields for the OH + MPAN reaction at T = 300 °K and P = 760 Torr. MPAN–OH, HOMPAN, MAE–NO_3, and HMML–NO_3 were subject to both forward and reverse reactions as well as energy-transferring thermalization collisions with the bath gas N_2. Further details concerning the VARIFLEX calculations can be found in the *SI Text*. Using the computed value of –1.80 kcal·mol^{-1} for the TS_2 transition state energy, the total rate constant using VARIFLEX was calculated to be 5.69×10^{-12} cm^3·molecule^{-1}·s^{-1}. This value differs significantly from the experimental value of $3.2 \pm 0.8 \times 10^{-11}$ cm^3·molecule^{-1}·s^{-1} at T = 275 °K reported by Orlando et al. (18), who noted their measured rate constant was expected to vary little from the value at 300 °K. Recent VARIFLEX calculations of rate constants for OH addition to hydrocarbons containing carbon double bonds have revealed similar differences. Greenwald et al. (34) observed for the OH + ethene addition reaction that decreasing the energy of the transition state analogous to TS_2 by 1.0 kcal·kmol^{-1}, which is within the expected accuracy of their ab initio calculations, results in good agreement with experimental data between 300 and 400 °K. A similar approach was adopted by Zador et al. (35) in their computational investigations of the OH + propene addition reaction. Consequently, the TS_2 transition state energy in the current study was adjusted to –2.80 kcal·mol^{-1} based on the reported improvements in rate constant predictions, and the VARIFLEX calculation was repeated, yielding a rate constant of 3.00×10^{-11} cm^3·molecule^{-1}·s^{-1}, in good agreement with the experimental value. We note, however, that the change in TS_2 does not significantly impact the product yields (*SI Text*). Using the revised TS_2 transition state energy and neglecting the MPAN–OH van der Waals complex because of its shallow energy minimum and low molar yield coefficient MPAN–OH = -3.10×10^{-7}, our calculations suggest the reaction mechanism, with its molar-based product yields, can be expressed as:

$$\mathrm{OH + MPAN \rightarrow 0.19\,HOMPAN + 0.21MAE\text{--}NO_3} + 0.57\,\mathrm{HMML\text{--}NO_3 + 0.03HAC\text{--}CO\text{--}NO_3}. \quad [1]$$

The VARIFLEX-derived estimate of 0.21 for the yield for MAE is within the range of 0.18–0.32 obtained in the chamber-based method. The major pathway for formation of MAE is the addition of OH radical to MPAN forming the chemically activated HOMPAN adduct. NO_3 then leaves HOMPAN by way of the rate-determining transition state TS_3, followed by a hydrogen atom transfer and formation of an epoxide (see Movie S1 for the calculated reaction). HMML warrants discussion as a potentially significant contributor to SOA as a consequence of its molar yield of 0.57. As a class, α-lactones are highly labile compounds that have not been observed under conditions relevant to the tropospheric environment (36, 37). Additionally, there are no reports of attempts to generate HMML or to determine its reaction products. 2-Oxooxirane, the unsubstituted structural analog of HMML that would be expected to have similar physicochemical properties, has been generated in the gas phase at 298 K and 100 Torr with a lifetime of ~150 μs (38). The short lifetime of 2-oxooxirane and the data available on α-lactones might argue against HMML as a major source of SOA; however, more work is needed to understand if HMML is an SOA precursor. Under atmospheric conditions, thermalized HOMPAN will react with O_2 forming the associated peroxy radical that will undergo further reactions. Additional studies are needed to determine whether these products contribute to SOA formation.

Atmospheric Relevance and Abundance of MAE. The sampling apparatus used for detection of MAE in the smog chamber photooxidation of MACR was assembled outdoors in Chapel Hill, North Carolina, during summer 2012. The EIC at m/z 101 from UPLC/ESI-HR-Q-TOFMS analysis of the field sample in Fig. 2*C* shows a peak with a retention time and accurate mass identical to that obtained from the MACR photooxidation under high-NO_x conditions (Fig. 2*A*) and the MAE standard (Fig. 2*B*). Taken together with the EICs from the chamber studies, the field samples confirm the presence of MAE in the ambient urban atmosphere. The average daytime concentration of 0.34 μg·m^{-3} (0.21–0.75 μg·m^{-3}, n = 6) and nighttime concentration of 0.16 μg·m^{-3} (0.07–0.34 μg·m^{-3}, n = 6) for gas-phase atmospheric MAE is in accord with expectation for a photochemical oxidation pathway in an area of high isoprene emissions influenced by anthropogenic NO_x, and is strong evidence that MAE is an important intermediate in the high-NO_x photochemistry of isoprene.

Fig. S5 shows the diurnal profile of surface layer gaseous MAE from July 21 to August 20, 2006 predicted by CMAQ after incorporation of gas-phase MAE chemistry into the model. Concentrations of MAE are predicted to increase in the early morning and peak in the afternoon between 3 and 5 PM local time. The predicted concentrations of MAE vary significantly from day-to-day, with afternoon MAE concentrations ranging from 0.05 to 0.25 μg·m^{-3}. Noteworthy is the consistency between the CMAQ predicted magnitude and diurnal variation in MAE concentration and field observations from 2012 (Table S3).

Fig. 5 shows the estimated concentration of surface layer gaseous MAE over the continental United States predicted by CMAQ during one month (July 21 to August 20) in summer 2006 at 12 km × 12 km horizontal resolution. The highest MAE concentrations reflect locations with high isoprene emissions, as well as significant anthropogenic activity that can provide NO_x to convert isoprene to MPAN. Near Atlanta, Georgia, MAE concentrations average around 0.1 μg·m^{-3} and can reach up to 0.6 μg·m^{-3}. Southern California and areas near St. Louis, Missouri, are also predicted to experience relatively high levels of MAE. In general, concentrations of MAE are predicted to average 0.06–0.1 μg·m^{-3} across the southeast and near the Ohio River Valley.

Uncertainty in predictions of isoprene emissions arise because of local meteorology as well as the modeling algorithm used to parameterize the emission process. CMAQ simulations in this study use Biogenic Emissions Inventory System (BEIS) emissions (39), which can be a factor of 2 lower than Model of Emissions of Gases and Aerosols from Nature (MEGAN) (1) predictions (40). Thus, the gaseous MAE concentrations may be significantly higher than currently displayed in Fig. 5. Furthermore, an aerosol uptake pathway for MAE has not yet been implemented in the model. Uptake to the aerosol phase could extend the lifetime of MAE by suppressing gas-phase reaction with OH. In addition, uncertainty in NO_x predictions as a result of chemistry and emissions, reflected in a high bias in NO_2 for urban areas and low bias in rural areas (41) as well as underestimated NO_3 wet deposition (42) in CMAQ, could lead to differences between measured and observed MAE concentrations.

Atmospheric Implications. The results presented here strongly support MAE as the precursor of 2-MG, the ubiquitous SOA tracer of both isoprene and MACR photooxidation under high-

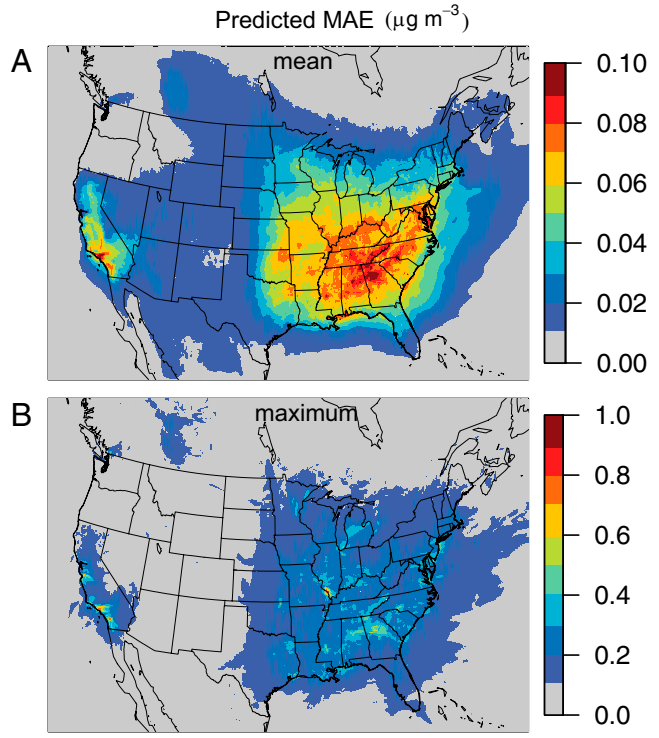

Fig. 5. July 21 to August 20, 2006 (*A*) mean and (*B*) maximum surface layer MAE concentration over the continental United States simulated by the updated CMAQ model.

NO_x conditions (10, 15). Reactive uptake of MAE by acidified sulfate seed aerosols and atmospheric aerosols (Fig. 3) points to MAE as the major and heretofore-unidentified precursor to SOA derived from isoprene photooxidation in the presence of NO_x. Furthermore, the distribution of the predicted mean gaseous MAE (Fig. 5*A*) matches the spatial patterns of enhanced summertime aerosol optical thickness over the southeastern United States observed by Goldstein et al. (43) (see *SI Text* for spatial distribution of other isoprene-derived high-NO_x products), likely linking our observations with the dominant summertime regional aerosol and the importance of biogenic volatile organic compound–anthropogenic interactions in radiative forcing in climate models. Taken together with the recent detection of isoprene epoxydiols under low-NO conditions (9–11), identification of MAE also implies epoxides derived from the oxidation of isoprene play a major role as SOA precursors. With respect to MAE, consistency between the predicted and chamber-based values for the yield of MAE as well as between observed ambient MAE levels and the CMAQ predictions are encouraging, and in accord with a contribution of MAE to SOA. However, additional work to develop a robust database of laboratory measurements of the OH + MPAN rate constant and product yields is needed to fully evaluate the proposed mechanism. Further investigation of the heterogeneous chemistry of MAE is also needed to elucidate the complex gas-particle interactions necessary to understand the kinetics and chemical fate of MAE under different atmospheric conditions, such as aerosol composition, liquid water content, and aerosol acidity.

Materials and Methods

MACR/NO_x Photooxidation Experiments. MACR/NO_x photooxidation experiments were carried out in a fixed volume 120 m^3 Teflon film environmental irradiation chamber, located on the roof of the University of North Carolina at Chapel Hill (UNC) Gillings School of Global Public Health. Initial conditions for each experiment consisted of 1 ppmv MACR, 0.2 ppmv NO, and 0.4 ppmv NO_2. No seed aerosol was injected into the chamber. All reactants were injected into the chamber before sunrise. Measurements from both gas and particle phases were taken periodically until sunset. Detailed operating conditions for chemical and physical monitoring of the chamber have been previously described (44). To detect gaseous MAE formation, chamber air was continuously drawn through two fritted-glass bubblers in series at a sampling flow rate of ~1 L·min^{-1}. Bubbler samples were collected in ethyl acetate cooled in an ice bath. Teflon membrane filters (Pall Life Science, 47 mm diameter, 1.0 μm pore size) were installed in front of the inlet to the glass bubblers to ensure collection of gas-phase MAE only. Bubbler samples were collected hourly throughout the course of experiments and analyzed immediately by UPLC/ESI-HR-Q-TOFMS (Agilent 6500 Series) operated in the negative (–) ion mode. We directly injected 50 μL aliquots from the bubbler samples onto the UPLC/ESI-HR-Q-TOFMS without additional treatment, and quantified with an authentic MAE standard. Details of UPLC/(–)ESI-HR-TOFMS operating conditions and procedures are described elsewhere (21). The detection limit of MAE by UPLC/(–)ESI-HR-TOFMS was 5 pg·μL^{-1}, based on signal-to-noise ratios > 3:1, and the uncertainty was ~3%.

Reactive Uptake Studies Using MAE. Authentic MAE was synthesized according to procedures described in the *SI Text* and Fig. S6. The synthetic standard was characterized by NMR and UPLC/(–)ESI-HR-Q-TOFMS for confirmation of structure and purity (Figs. S7–S9). The purity of MAE was determined to be ~99%. Reactive uptake of MAE onto preexisting seed aerosols was examined in the UNC 10 m^3 flexible Teflon indoor chamber. Details of this chamber have been described previously (11). A scanning electrical mobility sizing (SEMS) system (Brechtel Manufacturing Inc.) equipped with a cylindrical-geometry differential mobility analyzer and a mixing condensation particle counter was used to measure aerosol size distributions. Experiments were conducted with 300 ppbv MAE to ensure collection of sufficient SOA mass for off-line chemical analysis of reaction products. Aerosol samples were collected on Teflon membrane filters (Pall Life Science, 47 mm diameter, 1.0 μm pore size) at a sampling flow rate of ~20 L·min^{-1} for 2 h. For each experiment, two Teflon filters were stacked in the filter holder. Front filters were collected to examine particle-phase reaction products. The back filters served to correct for absorption of gaseous MAE; however, no gaseous MAE was found to absorb. All experiments were carried out under dark and dry conditions (relative humidity < 5%) at constant temperature (20–25 °C). Control experiments, including clean chamber, MAE only, and seed aerosol (acidic and neutral seed) only, were performed to rule out artifacts. Filters collected from these experiments revealed no MAE-derived SOA constituents.

Theoretical Calculations. All GAUSSIAN 2009, NEB, DIMER, and VARIFLEX calculations were run on an IBM iDataPlex cluster with six login nodes, with 160 compute nodes for running batch jobs, located in the National Computer Center on the US Environmental Protection Agency campus in Research Triangle Park, North Carolina. Each login node has two quad-core Intel Xeon ×5550 processors and 48 GB of memory (6 GB/core), while each compute node has two quad-core Intel Xeon ×5550 processors and either 32 GB or 48 GB of memory (4-6 GB/core). The Intel Xeon ×5550 processors operate at 2.66 GHz. Details of our VARIFLEX calculations are described in the *SI Text*.

Ambient Gas and Fine Aerosol Collection and Analyses. Ambient gas samples were collected in Chapel Hill, North Carolina, during summer 2012. The sampling site was located on the roof of the UNC Gillings School of Global Public Health building. Daytime (09:30–19:30, local time) and nighttime (20:30–06:30, local time) samples were collected. Samples were collected and analyzed in the same manner as gaseous samples collected from outdoor smog chamber studies, and quantified with an authentic MAE standard by UPLC/(–)ESI-HR-TOFMS. Archived ambient fine aerosol samples collected during the summer 2008 Mini-Intensive Gas and Aerosol Study (AMIGAS) in Atlanta, Georgia, at the Jefferson Street site were also analyzed. A detailed description of the sampling site and collocated measurements is provided elsewhere (45). Aerosol sample analysis is described in the *SI Text*.

Regional Chemical Transport Model Simulations. CMAQ Model v5.01 (46, 47) with the SAPRC07 chemical mechanism (48, 49) and isoprene updates (50) was further expanded to explicitly track peroxyacyl radicals from MACR oxidation, isoprene-derived MPAN, and later-generation MPAN oxidation products, including MAE and HMML to estimate ambient concentrations of MAE over the continental United States The yields and rate constant for the four MPAN product channels follow the yields estimated through computational chemistry in reaction Eq. **1** (see *SI Text* for additional documentation).

ACKNOWLEDGMENTS. Richard Kamens, Elias Rosen, Glenn Walters, and Denis Fedor are gratefully acknowledged for their assistance in the design and construction of the University of North Carolina at Chapel Hill (UNC) indoor smog chamber. The authors thank Rodney Weber and Xiaolu Zhang for providing 2008 Mini-Intensive Gas and Aerosol Study $PM_{2.5}$ filter samples. The authors also thank Bill Hutzell, Rob Pinder, Jose L. Jimenez, Joel Thornton, Douglas Worsnop, and Manjula Canagaratna for useful discussions. The US Environmental Protection Agency through its Office of Research and Development collaborated in the research described here. It has been subjected to the Agency's administrative review and approved for publication. This research was supported in part by the National Institute of Environmental Health Sciences (P30ES010126). Y.-H.L. and J.D.S. were supported in part by the Electric Power Research Institute. Y.-H.L. acknowledges a Dissertation Completion Fellowship from the UNC Graduate School. M.A. and S.H.B. were supported by the National Science Foundation Graduate Research Fellowship Program and Fulbright Presidential Fellowship Program, respectively. The University of North Carolina at Chapel Hill's Libraries provided support for open access publication.

1. Guenther A, et al. (2006) Estimates of global terrestrial isoprene emissions using MEGAN (Model of Emissions of Gases and Aerosols from Nature). *Atmos Chem Phys* 6(11):3181–3210.
2. Atkinson R, Arey J (2003) Gas-phase tropospheric chemistry of biogenic volatile organic compounds: A review. *Atmos Environ* 37(Suppl 2):197–219.
3. Chameides WL, Lindsay RW, Richardson J, Kiang CS (1988) The role of biogenic hydrocarbons in urban photochemical smog: Atlanta as a case study. *Science* 241(4872): 1473–1475.
4. Claeys M, et al. (2004) Formation of secondary organic aerosols through photooxidation of isoprene. *Science* 303(5661):1173–1176.
5. Edney EO, et al. (2005) Formation of 2-methyl tetrols and 2-methylglyceric acid in secondary organic aerosol from laboratory irradiated isoprene/NO_x/SO_2/air mixtures and their detection in ambient $PM_{2.5}$ samples collected in the eastern United States. *Atmos Environ* 39(29):5281–5289.
6. Kroll JH, Ng NL, Murphy SM, Flagan RC, Seinfeld JH (2005) Secondary organic aerosol formation from isoprene photooxidation under high-NO_x conditions. *Geophys Res Lett* 32(18):L18808.
7. Kroll JH, Ng NL, Murphy SM, Flagan RC, Seinfeld JH (2006) Secondary organic aerosol formation from isoprene photooxidation. *Environ Sci Technol* 40(6):1869–1877.
8. Surratt JD, et al. (2006) Chemical composition of secondary organic aerosol formed from the photooxidation of isoprene. *J Phys Chem A* 110(31):9665–9690.
9. Paulot F, et al. (2009) Unexpected epoxide formation in the gas-phase photooxidation of isoprene. *Science* 325(5941):730–733.
10. Surratt JD, et al. (2010) Reactive intermediates revealed in secondary organic aerosol formation from isoprene. *Proc Natl Acad Sci USA* 107(15):6640–6645.
11. Lin Y-H, et al. (2012) Isoprene epoxydiols as precursors to secondary organic aerosol formation: Acid-catalyzed reactive uptake studies with authentic compounds. *Environ Sci Technol* 46(1):250–258.
12. Henze DK, Seinfeld JH (2006) Global secondary organic aerosol from isoprene oxidation. *Geophys Res Lett* 33(9):L09812.
13. Carlton AG, Wiedinmyer C, Kroll JH (2009) A review of Secondary Organic Aerosol (SOA) formation from isoprene. *Atmos Chem Phys* 9(14):4987–5005.
14. Carlton AG, Pinder RW, Bhave PV, Pouliot GA (2010) To what extent can biogenic SOA be controlled? *Environ Sci Technol* 44(9):3376–3380.
15. Hallquist M, et al. (2009) The formation, properties and impact of secondary organic aerosol: Current and emerging issues. *Atmos Chem Phys* 9(14):5155–5236.
16. Chan AWH, et al. (2010) Role of aldehyde chemistry and NO_x concentrations in secondary organic aerosol formation. *Atmos Chem Phys* 10(15):7169–7188.
17. Tuazon EC, Atkinson R (1990) A product study of the gas-phase reaction of methacrolein with the OH radical in the presence of NOx. *Int J Chem Kinet* 22(6):591–602.
18. Orlando JJ, Tyndall GS, Paulson SE (1999) Mechanism of the OH-initiated oxidation of methacrolein. *Geophys Res Lett* 26(14):2191–2194.
19. Tuazon EC, Atkinson R (1990) A product study of the gas-phase reaction of isoprene with the OH radical in the presence of NO_x. *Int J Chem Kinet* 22(12):1221–1236.
20. Kjaergaard HG, et al. (2012) Atmospheric fate of methacrolein. 2. Formation of lactone and implications for organic aerosol production. *J Phys Chem A* 116(24):5763–5768.
21. Zhang H, Surratt JD, Lin Y-H, Bapat J, Kamens RM (2011) Effect of relative humidity on SOA formation from isoprene/NO photooxidation: enhancement of 2-methylglyceric acid and its corresponding oligoesters under dry conditions. *Atmos Chem Phys* 11(13): 6411–6424.
22. Zhang H, et al. (2012) Secondary organic aerosol formation from methacrolein photooxidation: Roles of NO_x level, relative humidity and aerosol acidity. *Environ Chem* 9(3):247–262.
23. Kleindienst TE, et al. (2007) Estimates of the contributions of biogenic and anthropogenic hydrocarbons to secondary organic aerosol at a southeastern US location. *Atmos Environ* 41(37):8288–8300.
24. Jaoui M, et al. (2008) Formation of secondary organic aerosol from irradiated α-pinene/toluene/NOx mixtures and the effect of isoprene and sulfur dioxide. *J Geophys Res* 113(D9):D09303.
25. Birdsall AW, Zentner CA, Elrod MJ (2012) Study of the kinetics and equilibria of the oligomerization reactions of 2-methylglyceric acid. *Atmos Chem Phys Discuss* 12(11): 30039–30080.
26. Frisch MJ, et al. (2009) *Gaussian 09 Revision A. 1* (Gaussian Inc., Wallingford, CT).
27. Mills G, Jónsson H, Schenter GK (1995) Reversible work transition state theory: Application to dissociative adsorption of hydrogen. *Surf Sci* 324(2-3):305–337.
28. Alfonso DR, Jordan KD (2003) A flexible nudged elastic band program for optimization of minimum energy pathways using ab initio electronic structure methods. *J Comput Chem* 24(8):990–996.
29. Heyden A, Bell AT, Keil FJ (2005) Efficient methods for finding transition states in chemical reactions: Comparison of improved dimer method and partitioned rational function optimization method. *J Chem Phys* 123(22):224101.
30. Papajak E, Leverentz HR, Zheng J, Truhlar DG (2009) Efficient Diffuse Basis Sets: cc-pV x Z+ and maug-cc-pV x Z. *J Chem Theory Comput* 5(5):1197–1202.
31. Klippenstein SJ, Miller JA (2002) From the time-dependent, multiple-well master equation to phenomenological rate coefficients. *J Phys Chem A* 106(40):9267–9277.
32. Miller JA, Klippenstein SJ (2006) Master equation methods in gas phase chemical kinetics. *J Phys Chem A* 110(36):10528–10544.
33. Klippenstein SJ, et al. (2008) *VARIFLEX, version 2.0* (Argonne National Laboratory, Argonne, IL).
34. Greenwald EE, North SW, Georgievskii Y, Klippenstein SJ (2005) A two transition state model for radical-molecule reactions: A case study of the addition of OH to C2H4. *J Phys Chem A* 109(27):6031–6044.
35. Zádor J, Jasper AW, Miller JA (2009) The reaction between propene and hydroxyl. *Phys Chem Chem Phys* 11(46):11040–11053.
36. L'abbé G (1980) Heterocyclic analogues of methylenecyclopropanes. *Angew Chem Int Ed Engl* 19(4):276–289.
37. Wheland R, Bartlett PD (1970) α-Lactones from diphenylketene and di-*tert*-butylketene. *J Am Chem Soc* 92(20):6057–6058.
38. Chen S-Y, Lee Y-P (2010) Transient infrared absorption of t-$CH_3C(O)OO$, c-$CH_3C(O)OO$, and alpha-lactone recorded in gaseous reactions of CH_3CO and O_2. *J Chem Phys* 132(11):114303–114311.
39. Carlton AG, et al. (2010) Model representation of secondary organic aerosol in CMAQv4.7. *Environ Sci Technol* 44(22):8553–8560.
40. Carlton AG, Baker KR (2011) Photochemical modeling of the Ozark isoprene volcano: MEGAN, BEIS, and their impacts on air quality predictions. *Environ Sci Technol* 45(10): 4438–4445.
41. Appel KW, et al. (2011) A multi-resolution assessment of the Community Multiscale Air Quality (CMAQ) model v4.7 wet deposition estimates for 2002–2006. *Geosci Model Dev* 4(2):357–371.
42. Allen DJ, et al. (2012) Impact of lightning-NO on eastern United States photochemistry during the summer of 2006 as determined using the CMAQ model. *Atmos Chem Phys* 12(4):1737–1758.
43. Goldstein AH, Koven CD, Heald CL, Fung IY (2009) Biogenic carbon and anthropogenic pollutants combine to form a cooling haze over the southeastern United States. *Proc Natl Acad Sci USA* 106(22):8835–8840.
44. Ebersviller S, et al. (2012) Gaseous VOCs rapidly modify particulate matter and its biological effects – Part 1: Simple VOCs and model PM. *Atmos Chem Phys* 12(24): 12277–12292.
45. Hansen DA, et al. (2003) The southeastern aerosol research and characterization study: Part 1-overview. *J Air Waste Manag Assoc* 53(12):1460–1471.
46. Byun D, Schere KL (2006) Review of the governing equations, computational algorithms, and other components of the models-3 Community Multiscale Air Quality (CMAQ) modeling system. *Appl Mech Rev* 59(1-6):51–77.
47. Foley KM, et al. (2010) Incremental testing of the Community Multiscale Air Quality (CMAQ) modeling system version 4.7. *Geosci Model Dev* 3(1):205–226.
48. Carter WPL (2010) Development of the SAPRC-07 chemical mechanism. *Atmos Environ* 44(40):5324–5335.
49. Hutzell WT, Luecken DJ, Appel KW, Carter WPL (2012) Interpreting predictions from the SAPRC07 mechanism based on regional and continental simulations. *Atmos Environ* 46(0):417–429.
50. Xie Y, et al. (2012) Understanding the impact of recent advances in isoprene photooxidation on simulations of regional air quality. *Atmos Chem Phys Discuss* 12(10): 27173–27218.